A computational driver model to predict driver control at unsignalised intersections

N.B. When citing this work, cite the original published paper.

(article starts on next page)

A Computational Driver Model to Predict Driver Control at Unsignalised Intersections

CHRISTIAN-NILS BODA, **ESKO LEHTONEN**, **AND MARCO DOZZA**
Department of Mechanics and Maritime Sciences, Chalmers University of Technology, 412 96 Gothenburg, Sweden
Corresponding author: Christian-Nils Boda (christian-nils.boda@chalmers.se)

ABSTRACT The number of cyclists fatally struck when crossing a driver's travel path at an unsignalised intersection has been stable in recent years, indicating that more effort should be made to improve safety in this specific conflict scenario. The most recent safety systems help drivers avoid collisions with cyclists, but improving cyclist safety further requires resolving challenges unique to bicycles and cyclists. In this paper we propose a predictive computational model of driver behaviour in the intersection scenario. Although a handful of studies have focused on describing driver behaviour in this scenario, no computational model that can predict driver control can be found in the literature. The proposed model is based on a biofidelic human sensorimotor-control modelling framework. Two visual cues were used: 1) optical longitudinal looming and 2) projected post-encroachment time between the bicycle and the car. The model was optimised using data from a test-track study in which participants were asked to drive through an intersection where a cyclist would cross their travel path. The performances of the model were evaluated by comparing the simulated driver-control process with the observed control behaviour for each trial using a leave-one-out cross-validation process. The results show that the model performed rather well, reproducing braking controls and kinematics that were similar to the observations. The extent to which the model could be used by safety systems' threat-assessment algorithms is discussed. Future research to improve the model's performances is suggested.

INDEX TERMS Predictive computational model, accumulator model, crossing, driver behaviour, cyclist, test-track data.

I. INTRODUCTION

As the interest in cycling continues to grow because of health and environmental benefits, so does the number of conflicts between motorists and cyclists. The European crash statistics database shows that the proportion of cyclist fatalities compared to all road fatalities has been increasing year after year [1]. Developing countermeasures to change this trend is an important matter. In fact, safety systems—such as automated emergency braking (AEB) or forward collision warning (FCW)—designed for crossing-cyclist scenarios are now being installed in cars. As a result, the European new car assessment program (Euro NCAP) now assesses AEB system functionality when the car is on a collision course with a crossing cyclist [2]. The performance of the threat-assessment algorithms implemented in safety systems

The associate editor coordinating the review of this manuscript and approving it for publication was Arianna Dulizia.

(independent of their assessment domain) depends on accurately predicting drivers' intent [3]. Unfortunately, very few driver behaviour models address crossing-cyclist scenarios. Two exceptions are the model by Silvano *et al.*, who developed a probabilistic model that predicts whether a driver will decide to yield for a crossing cyclist [4]. In the second, Bella *et al.* presented a set of descriptive statistics related to driver behaviour in a simulator environment when a cyclist was crossing the travel path. Although their work focused on the effect of different infrastructure designs on the drivers' control, the results provide valuable information about how drivers control their car [5]. While both models predict some elements of driver control, they do not predict continuous driver control. Recently, we proposed a model that predicts when drivers initiate braking, given the moment when they see the cyclist for the first time [6]. This brake-onset prediction (BOP) model is particularly relevant for warning systems, since it can more precisely determine whether a

warning is relevant when the driver fails to control the car according to the situation. The BOP model is a first step towards a complete predictive model, but it has several limitations: 1) the model always predicts that the driver will initiate braking; 2) it does not take into account the encroachment sequence—if the cyclist and the car pass through the intersection at very different times, drivers are less likely to brake; and 3) it predicts neither the level of braking nor the entire braking control sequence that follows brake initiation (i.e., as with the two previously cited models, it does not model a continuous control signal).

In the BOP study, we speculated that braking initiation is due to the accumulation of evidence for the need to brake due to visual looming (the optical expansion of an object on the retina). To test this hypothesis, we implemented a computational model using Markkula *et al.*'s framework based on accumulator models, which use perceptual cues as input [7]. Accumulator models were developed by neuroscientists to explain how evidence that accumulates from perceptual cues could initiate a control action [8]. This framework has already been used to model driver control in different situations. For example, Svärd *et al.* used the framework to predict braking control in rear-end scenarios [9]. The original designers of the framework used it to implement a steering control model [7], adapting the continuous steering model of Salvucci and Gray [10]. In a subsequent study, they also demonstrated that non-visual cues could be integrated into their framework, showing that vestibular cues have an important role in driver control in slalom tasks [11]. The present paper is the first attempt to extend this framework to model driver control in crossing scenarios. The choice of perceptual cues is crucial to make the model comparable to human control. In previous implementations (i.e., rear-end scenarios [9], [12]), the looming cue was used as input to the model. Similarly, our implementation also uses looming as an excitatory cue which elicits the need for braking. However, as previously used, the cue does not apply in crossing scenarios, since it represents the optical expansion of the lead vehicle. Instead, we used the longitudinal looming of the intersection point (i.e., the intersection point between the bicycle's and the car's travel paths). This cue is already used in the literature to model human locomotion [13]. An intervention by the driver in a crossing scenario cannot be based only on this excitatory cue, however; if the cyclist crosses the intersection well before or after the car, the drivers may not brake at all. As a consequence, a cue that indicates whether the car is on a collision course or not is also required. In the human locomotion literature, the bearing angle (the angle between the direction of travel and a moving target or collision object) has been recognised as a relevant cue. If the bearing angle to an object remains constant, a collision will happen as long as the distance to the object also decreases [14], [15]: to avoid a collision, the bearing angle change rate must be non-zero. This concept was implemented by Fajen in a recent mathematical model [13], which predicts the possible heading and speed that humans can adopt to avoid a moving obstacle. As the model

illustrates, it is not enough to know the bearing angle's change rate, because the chance of collision also depends on the distance to the intersecting object. The speed and heading calculations are based on the time necessary for the human observer to pass before or after the obstacle (note that the time is partly derived from the bearing angle change rate). This time is related to the post-encroachment time (PET) metric used to study traffic conflict [16], with the difference that the former is derived using optical angles. Because PET accounts for both road users' physical envelopes while bearing angle does not, the former was chosen as the inhibitory cue in our implementation. The cue is inhibitory because it provides evidence that there is no need for braking. Note that PET is compatible with the constant bearing angle strategy [14], [15]: when PET is equal to zero, the observer is on a collision course with the obstacle or road user. The implemented model's performance was analysed to test the hypothesis that looming and PET suffice to explain drivers' control when a cyclist crosses their travel path.

The objectives of the study were: 1) to devise a computational driver model that could be used for practical applications (e.g., threat-assessment algorithms of safety systems), 2) to assess the prediction performances of the model, and 3) to test the hypothesis that longitudinal looming and post-encroachment time cues drive the drivers' response process in crossing-cyclist scenarios.

II. METHODOLOGY
A. DATA COLLECTION
1) PARTICIPANTS
Forty-four employees of Autoliv AB, Sweden, were recruited. The participants were required to have a valid driving license and be older than 25. Because three participants did not follow the instructions their data were excluded from analysis. Therefore, the final dataset included data from 41 drivers, of whom 32% were female. The average age of the participants was 41.8 years, with a standard deviation of 10.4 years. The average time that the participants had their driving license was 23.3 years, with a standard deviation of 10.5 years. More information about this dataset can be found in our paper [6].

2) EXPERIMENTAL SETUP
The data collection was carried out on the Carson City test track [17], Vårgårda, Sweden. The participants were asked to drive through an intersection in which a (robot) cyclist, coming from the right side, might cross their path. The participants started to drive 180 m away from the intersection point. They were instructed to reach a target speed before arriving at a photo-cell sensor that would trigger the cyclist, hidden behind a wall at the beginning of each run. A balloon car was placed in the opposite lane 30 m in front of the intersection point to simulate oncoming traffic, limiting participants' steering avoidance. The setup is represented in Figure 1.
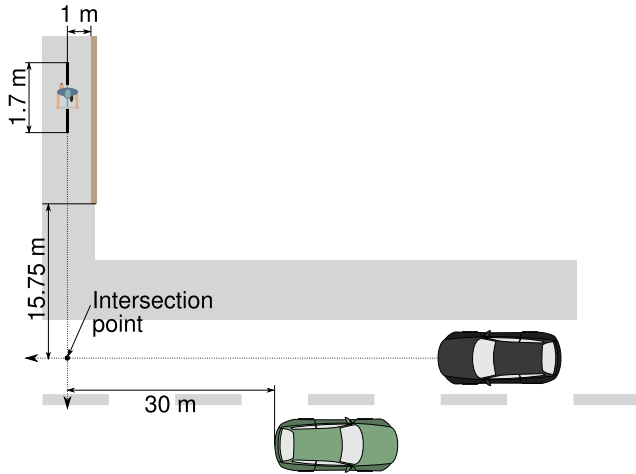
FIGURE 1. Layout of the experiment. The car driven by the participants (black car) approached an unsignalised intersection where a robot cyclist crossed the participants' travel path from their near side. A balloon car (green car) was parked in the opposite lane 30 m away from the intersection point, in order to limit drivers' ability to steer away.

The data from the car and bicycle kinematics (positions, speeds, accelerations, etc.) were collected at 100 Hz using a VBOX 3 RTK (Racelogic Ltd.). Additionally, the car's gas and brake pedal positions were recorded using two-wire potentiometers.

3) EXPERIMENTAL PROTOCOL

In total, 20 trials were recorded for each participant after a test drive. In four of them the cyclist did not appear at the intersection at all. We included these trials to make the experiment less predictable, hopefully slowing down the driver's adaptation. The 16 remaining trials resulted from combining the four factors: 1) the car's target speed (30 or 50 km/h), 2) the cyclist's speed (10 or 20 km/h), 3) the encroachment sequence at the intersection (bicycle passes before the car, potential 50%-overlap crash, and car passes before the bicycle), and 4) the cyclist crosses the road or brakes before it. Twelve trials resulted from the full factorial design ($2 \times 2 \times 3$) of the first three factors, and in the four remaining trials the bicycle came to a rest before reaching the right edge of the main road. The configuration of the 16 trials is summarised in Table 1. The 16 trials were randomised for each participant.

Further details of the experimental protocol can be found in the previously mentioned paper [6].
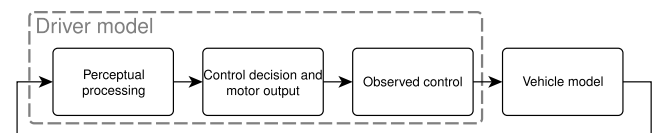
B. IMPLEMENTATION OF MODELS

This section describes the implementation of the driver model using Markkula *et al.*'s framework [7]. For further details on the framework and on its ecological roots, we refer the reader to the original paper.

The framework flow can be divided into four blocks [7] as represented in Fig. 2: 1) perceptual processing, 2) control decision and motor output, 3) observed control, and 4) vehicle

TABLE 1. Factorial design for each trial.

Trial number	Cyclist speed	Car speed	Encroachment sequence	Cyclist braking
1	20	30	bicycle passes first	no
2	20	30	50%-overlap crash	no
3	20	30	car passes first	no
4	20	50	bicycle passes first	no
5	20	50	50%-overlap crash	no
6	20	50	car passes first	no
7	10	30	bicycle passes first	no
8	10	30	50%-overlap crash	no
9	10	30	car passes first	no
10	10	50	bicycle passes first	no
11	10	50	50%-overlap crash	no
12	10	50	car passes first	no
13	20	30	bicycle passes first	yes
14	20	50	50%-overlap crash	yes
15	10	30	bicycle passes first	yes
16	10	50	50%-overlap crash	yes

FIGURE 2. Overall diagram of the implemented framework (adapted from Markkula *et al.* [7]).

model. The implementation of each block is described in the following sub-sections. The first three blocks comprise the driver model; a more detailed diagram can be found in Fig. 3. Examples of signals generated by the driver model are presented in Fig. 4.

1) PERCEPTUAL PROCESSING

The perceptual processing block computes two quantities from the two perceptual cues. The first cue is the longitudinal looming (τ^{-1}), the optical angle between the driver's line of sight and the future intersection point of the two road users' travel paths, from which the excitatory perceptual quantity ($P_{excitatory}$) is derived.

The longitudinal looming, τ^{-1}, is defined as

$$\tau^{-1} = \dot{\gamma}/\gamma, \qquad (1)$$

where γ is defined as the angle between the intersection point and the line of sight (see Fig. 5.a). This definition was borrowed from Fajen's model (see [13]). In the simulations, the height of the drivers' eyes was set to 1.2 m above the ground. Note that this assumption may be a source of discrepancy between the actual and simulated values of τ^{-1} because the actual drivers' eyes may not have been exactly 1.2 m above the ground.
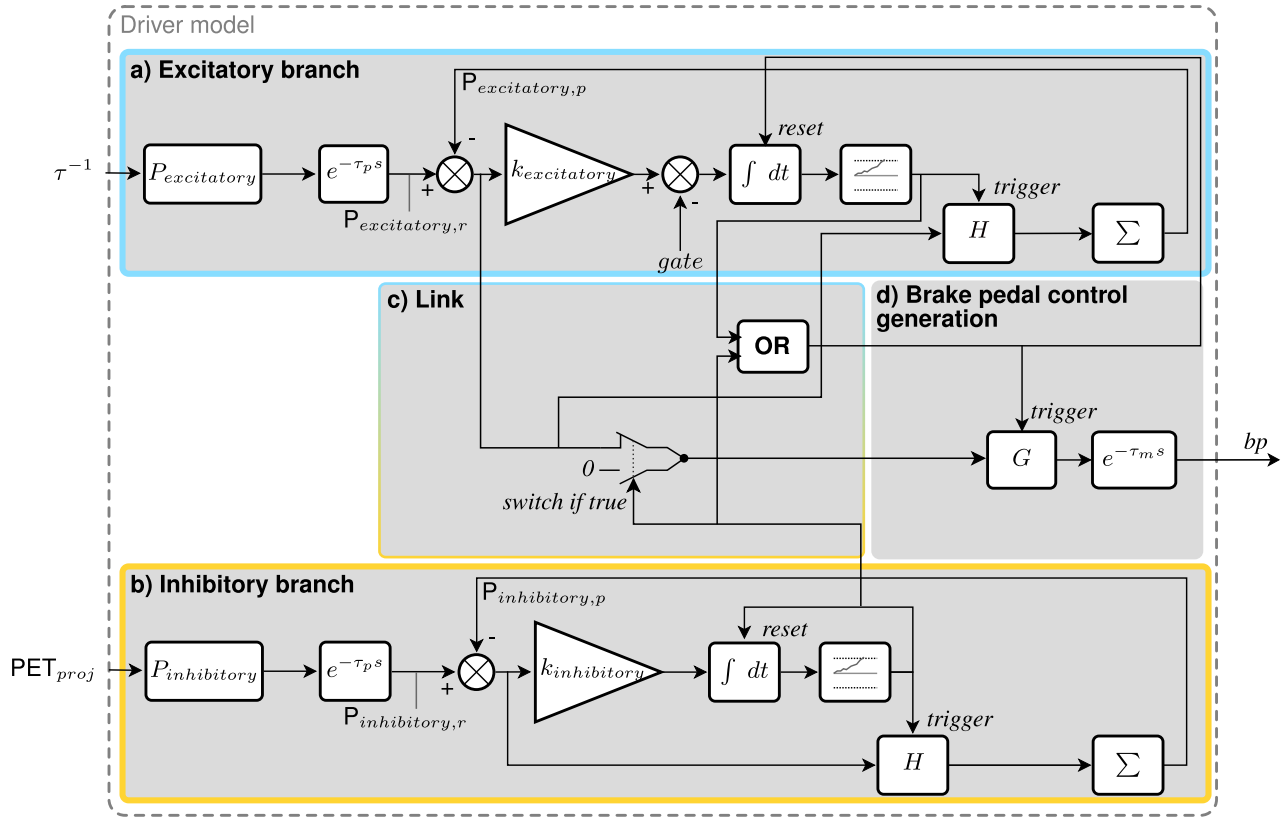
FIGURE 3. An illustration of the driver model based on Markkula *et al.*'s framework. The excitatory part of the model is at the top and the inhibitory part is at the bottom.

The inhibitory perceptual quantity ($P_{inhibitory}$) was derived from the second implemented cue PET_{proj}, defined as the projected PET between the bicycle and the car. This time is the projected time from the moment one of the road users exits the conflict zone (see Fig. 5.b) to the moment the other road user enters it, assuming constant speeds. Thus, three cases must be considered, depending on the projected encroachment sequence:

$$PET_{proj} = \begin{cases} t_{C,enters} - t_{B,exits}, & \text{if bicycle passes first} \\ t_{C,exits} - t_{B,enters}, & \text{if car passes first} \\ 0, & \text{otherwise,} \end{cases} \quad (2)$$

where t_C is the time related to the car, and t_B the time related to the bicycle.

The first perceptual quantity, ($P_{excitatory}$), is defined by

$$P_{excitatory}(t) = K_{excitatory} \times \tau^{-1}(t), \quad (3)$$

where $K_{excitatory}$ is a constant perceptual gain.

The second quantity, ($P_{inhibitory}$), is inhibitory. It is defined by

$$P_{inhibitory}(t) = -K_{inhibitory} \times |PET_{proj}(t)|, \quad (4)$$

where $K_{inhibitory}$ is a constant perceptual gain.

### 2) CONTROL DECISION AND MOTOR OUTPUT

This block can be broken down into four parts (see Fig. 3): a) *Excitatory branch*, b) *Inhibitory branch*, c) *Link*, and d) *Brake pedal control*. The first two contain accumulation models based on the excitatory and inhibitory cues (τ^{-1} and PET_{proj}), respectively. The third part, *Link*, connects both branches, giving priority to the inhibitory branch. Finally, the *Brake pedal control* part implements a motor-primitive-based algorithm which generates a continuous brake-pedal profile, given a brake-pedal deflection target.

a: EXCITATORY BRANCH

The excitatory evidence accumulator, $A_{excitatory}(t)$, is defined by

$$\frac{dA_{excitatory}(t)}{dt} = \Gamma[k_{excitatory}\epsilon_{excitatory}(t)], \quad (5)$$

where $k_{excitatory}$ is a constant gain, Γ is a gating function defined by Markkula *et al.* [7] (see Eq. 6), and $\epsilon_{excitatory}(t)$ is the error between $P_{excitatory,r}$ and the predicted excitatory perceptual quantity, $P_{excitatory,p}$. $P_{excitatory,r}$ is the quantity $P_{excitatory}$ with the addition of the perceptual delay (τ_p) set to 0.05 s (from Markkula *et al.* [7]). When $A_{excitatory}$ reaches the excitatory accumulation threshold (arbitrarily set to 1), a brake adjustment is initiated, $A_{excitatory}$ is reset to zero, and $P_{excitatory,p}$ is updated (see (7)). The gating function Γ
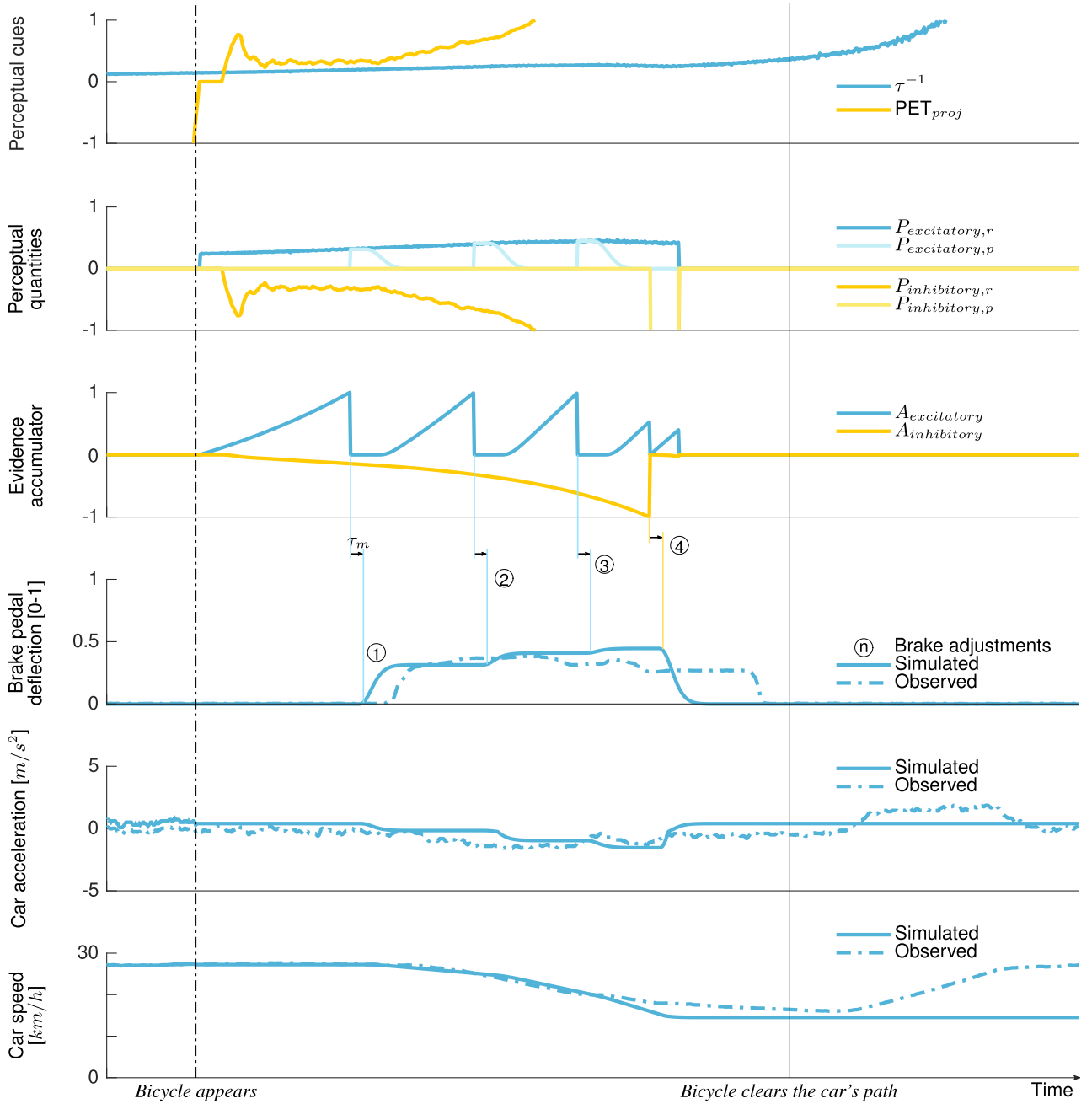
FIGURE 4. The signals generated by the driver model when replaying one trial extracted from the data. First row (starting at top): perceptual cues (τ^{-1} and PET_{proj}); second row: received and predicted perceptual quantities; third row: excitatory and inhibitory evidence accumulators; fourth row: simulated and observed brake pedal control; fifth row: car acceleration derived from the brake pedal deflection; and sixth row: car speed integrated from the car acceleration. From top to bottom, the rows match the process in the driver model, from the initial perception of cues to the final effect of the brake pedal action on the car kinematics. The vertical lines between the *Evidence accumulator* and the *Brake pedal deflection* plots show the relation between the brake adjustments and the moment when the accumulators reach either -1 (inhibitory) or 1 (excitatory). Finally, the time of the bicycle's appearance is shown by the long vertical dashed line and the time it cleared the car's path is shown by the long solid vertical line.

is defined by

$$\Gamma(\eta) = sgn(\eta) \cdot max(0, |\eta| - gate), \qquad (6)$$

where *gate* is a constant value. The quantity $P_{excitatory,p}$ is defined by

$$P_{excitatory,p}(t) = \sum_{i=1}^{n} \epsilon_{excitatory,i} H(t - t_i), \qquad (7)$$

where t_i is the time at the ith adjustment and $H(t)$ is a function that fulfills the following requirements:

$$\begin{cases} H(t) = 0, & \text{for } t \leq 0 \\ H(t) \rightarrow 1, & \text{for } t \rightarrow 0^+ \\ H(t) = 0, & \text{for } t \geq T_p, \end{cases} \qquad (8)$$

where T_p is the time when the control error is predicted to be corrected. As suggested by Markkula *et al.* [7], the $H(t)$
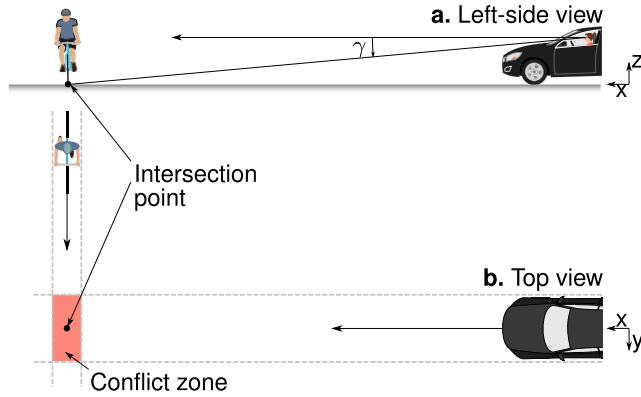
FIGURE 5. a. Left-side view of scenario (above in figure) shows γ, the angle between a horizontal line and the sight line from the driver's eyes to the intersection point of both road users' travel paths. b. Top view of scenario (below in figure) shows the conflict zone used to calculate the projected post-encroachment time, PET_{proj}.

function is defined as:

$$H(t) = \begin{cases} 0 & \text{for } t \leq 0 \\ 1 - G(t - \tau_p) & \text{for } t > 0, \end{cases} \quad (9)$$

where G is the kinematic motor-primitive function present in the *Brake pedal control generation* part. In the present implementation, G is defined as in (12) to (15) with the brake-deflection target T set to 1.

b: INHIBITORY BRANCH

The inhibitory branch shares the same structure as the excitatory branch, except that the inhibitory evidence accumulator, $A_{inhibitory}$, does not include a gating function:

$$\frac{dA_{inhibitory}(t)}{dt} = k_{inhibitory}\epsilon_{inhibitory}(t), \quad (10)$$

where $k_{inhibitory}$ is a constant gain. Analogous to the excitatory branch, $\epsilon_{inhibitory}(t)$ is the error between $P_{inhibitory,r}$ and the predicted inhibitory perceptual quantity, $P_{inhibitory,p}$. When $A_{inhibitory}$ reaches the inhibitory evidence accumulation threshold (arbitrarily set to -1), the release of the brake pedal is initiated, $A_{inhibitory}$ and $A_{excitatory}$ are reset to 0, and $P_{inhibitory,p}$ is updated:

$$P_{inhibitory,p}(t) = \sum_{i=1}^{n} \epsilon_{inhibitory,i} H(t - t_i). \quad (11)$$

c: LINK

The *Link* part, connecting the inhibitory and excitatory branches, initiates the brake-pedal adjustments and estimates their magnitudes. By design, the inhibitory branch is prioritised over the excitatory one. Two situations are possible:

- When $A_{inhibitory}$ reaches -1, the brake-control target is set to zero and brake-pedal release is initiated. Additionally, $A_{excitatory}$ is reset to zero via the *OR* gate.
- When $A_{excitatory}$ reaches 1, the control target is set to $P_{excitatory,r}$ and brake-pedal adjustment is initiated.
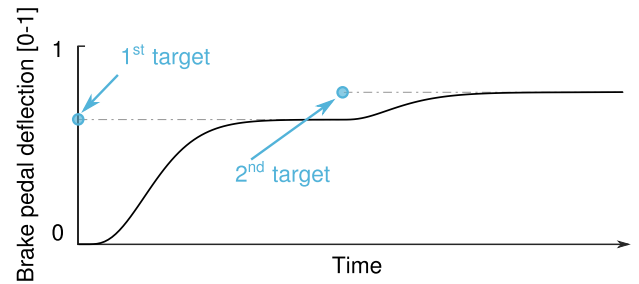
FIGURE 6. Example of brake-pedal control output from the motor-primitive function (*G*). Two successive brake-pedal adjustments are shown in the figure. The *G* function generates a continuous control signal, given the brake-pedal target, whenever a brake-pedal adjustment is initiated.

d: BRAKE-PEDAL CONTROL

The *brake pedal control* block, based on the function G, generates a continuous brake-pedal signal given a brake-pedal deflection target (see Fig. 6). The G function was derived from the algorithm proposed by Schaal *et al.* [18] and adapted from Dégallier Rochat's implementation[1] [19]. Our implementation used the MATLAB *ode45* function to solve differential equations, reducing execution time. The G function is a set of differential equations defined by (12) to (15) (using the same variable naming used by Dégallier Rochat [19]). The set of equations models one agonist muscle and one antagonist muscle ($i = 1$ and $i = 2$, respectively).

The activation signal v_i is the difference between the brake-pedal deflection target (where T equals both the deflection target for the agonist muscle and the opposite of the deflection target for the antagonist muscle) and the current brake-pedal target p:

$$\begin{cases} \Delta w_i = max(0, T - p) \\ \dot{v}_i = a_v(-v_i + \Delta w_i), \end{cases} \quad (12)$$

where the parameter a_v controls the rate of convergence of v_i. The velocity signal was generated by smoothing the activation signal v_i twice (i.e., with the smoothing functions x_i and y_i)

$$\begin{cases} \dot{x}_i = -a_x x_i + (v_i - x_i)c_0 \\ \dot{y}_i = -a_y y_i + (x_i - y_i)c_0, \end{cases} \quad (13)$$

where the parameters a_x and a_y control the rate of convergence of x_i and y_i, respectively, while the parameter c_0 sets the speed of the movement. The speed of the brake-pedal adjustment, z_i, is calculated by integrating y_i and using an auxiliary variable, r_i, to ensure that z_i has a motor-primitive shape (i.e., bell shape):

$$\begin{cases} \dot{r}_i = a_r(-r_i + (1 - r_i)bv_i) \\ \dot{z}_i = -a_z z_i + (y_i - z_i)(1 - r_i)c_0, \end{cases} \quad (14)$$

where the parameters a_r and b set the shape of z_i, and the parameter a_z controls its rate of convergence. Finally, the brake-pedal deflection, bp, is calculated by integrating the

[1]Retrieved from http://biorob2.epfl.ch/users/degallie/matlab_chap3.tar

speeds of the agonist and antagonist muscles ($i = 1$ and $i = 2$, respectively).

$$\dot{bp} = a_p(max(0, z_1) - max(0, z_2))c_0, \qquad (15)$$

where the parameter a_p controls the rate of convergence of the $\dot{bp}$.

Note that the parameters defined above were determined during the optimisation of the model (see next section).

The generated brake-pedal signal is then output from the block after a motor-delay time ($\tau_m = 0.1$ s).

3) OBSERVED CONTROL
Because the control (brake-pedal deflection) is directly observable, this block was not implemented in the driver model.

4) VEHICLE MODEL
The vehicle model generates the car's longitudinal kinematics, given the control signals from the driver model. The vehicle model was implemented as follows:

$$\ddot{x}(bp, \dot{x}) = \begin{cases} 0, & \text{if } \dot{x} = 0 \\ q_1 \times bp, & \text{if } \dot{x} > 0 \\ & \text{and } bp < \dfrac{g - q_2}{q_1 - q_2} \\ q_2 \times (bp - 1) - g, & \text{if } \dot{x} > 0 \\ & \text{and } bp \geq \dfrac{g - q_2}{q_1 - q_2}, \end{cases} \qquad (16)$$

where $\ddot{x}$ is the vehicle longitudinal acceleration (in m/s^2) given bp the brake-pedal deflection (ranging from 0 to 1), $\dot{x}$ is the vehicle speed (in m/s), q_1 and q_2 are the two coefficients defining the two distinct slopes of the model in approximation of an actual braking curve, and g is a constant equal to 9.81 m/s^2.

After the vehicle acceleration due to the brake-pedal action was calculated, the vehicle longitudinal position (x) and speed ($\dot{x}$) were calculated at every j step of the simulation using the following basic kinematics equations:

$$\begin{cases} \dot{x}_{j+1} = \ddot{x}_j \times \Delta t + \dot{x}_j \\ x_{j+1} = \ddot{x}_j \times \dfrac{\Delta t^2}{2} + \dot{x}_j \times \Delta t + x_j. \end{cases} \qquad (17)$$

Note that when the collected data were replayed, the car kinematics were modified to discard any original driver braking or accelerating control. That is, for each run, the car speed was set equal to the observed car speed when the bicycle became visible.

C. OPTIMISATION OF MODELS
This section describes how the parameters of the driver model and the vehicle model were optimised.

1) PERCEPTUAL PROCESSING
a: EXCITATORY BRANCH ($K_{excitatory}$)
The perceptual quantity of the excitatory branch defines the target of brake-pedal deflection when a braking action is triggered. Therefore, the optimisation process for finding $K_{excitatory}$ required determining the right amount of gain to create a brake-pedal deflection value ranging from 0 (fully released) to 1 (fully depressed), using τ^{-1}. A simple algorithm to detect the brake onset was used to determine the adjustments required to the actual observed brake signal. The value of τ^{-1} before the perceptual and motor delays (τ_p and τ_m) was extracted for each trial in which braking occurred. The amount of brake-pedal deflection after this first brake adjustment (bp_{BO}) was extracted for each trial. The perceptual gain $K_{excitatory}$ was then estimated by fitting a linear mixed-effect model, defined by (3) and including a random effect due to the drivers (the MATLAB function *fitlme* was used). As a consequence, the results describe driver-specific perceptual gains.

b: INHIBITORY BRANCH ($K_{inhibitory}$)
The inhibitory branch is not used to set a brake target; it merely triggers the brake-pedal release. Therefore, $K_{inhibitory}$ was arbitrarily set to 1. However, the accumulation gain, $k_{inhibitory}$, was tuned to make sure that the driver model reproduces a realistic brake-pedal release.

2) CONTROL DECISION AND MOTOR OUTPUT
a: EXCITATORY BRANCH ($k_{excitatory}$, gate)
The two parameters of the accumulator $A_{excitatory}$ were chosen so that the accumulator reaches a value of 1 when a brake-pedal adjustment is required. Because $P_{excitatory,p}$ is equal to zero for the brake onset, $\epsilon_{excitatory}$ was simply equated to $P_{excitatory,r}$, which was calculated for all the trials where a braking control occurred. The parameters $k_{excitatory}$ and *gate* were tuned using a non-linear mixed-effects model to include driver as a random effect. The MATLAB function *nlmefit* was used.

b: INHIBITORY BRANCH ($k_{inhibitory}$)
The inhibitory accumulator ($A_{inhibitory}$) was arbitrarily set to reach an accumulation threshold equal to -1. The gain in the perceptual quantity equation ($k_{inhibitory}$; see (4)) was determined by optimisation to fulfill the requirement for $A_{inhibitory}$ for the collected data.

There were two cases to consider in the collected data: i) the trials in which the driver braked, and ii) the others.

i) When the driver braked, the received perceptual quantity $P_{inhibitory,r}$ was computed with $k_{inhibitory}$ set to 1, considering PET_{proj} from the moment the bicycle started to be visible ($t_{visibility}$) to the moment when the driver made the decision to release the brake pedal (i.e., $\tau_p + \tau_m$ before the start of observed brake-pedal release).

ii) When the driver did not brake, $P_{inhibitory,r}$, with $k_{inhibitory}$ set to 1, was calculated from $t_{visibility}$ to

TABLE 2. Parameters used for G.

Parameter	a_p	a_r	a_v	a_x	a_y	a_z	b	c_0
Value	0.08	50.0	50.0	1	1	0.01	10	70

the moment when the excitatory branch's $A_{excitatory}$ would have reached 1. Because the driver did not brake, $A_{inhibitory}$ would have reached -1 when $A_{excitatory}$ reached 1, at the latest.

The $k_{inhibitory}$ gain was then estimated, using a linear mixed-effect model with the drivers as random effects (to minimise the error between -1 and the accumulator $A_{inhibitory}$, derived from the $P_{inhibitory}$ previously calculated). Because this optimisation was done at the first full release of the brake pedal, $P_{inhibitory,p}$ was negligible, so $\epsilon_{inhibitory}$ was simply equated to $P_{inhibitory,r}$.

c: MOTOR OUTPUT

First order Gaussians were fitted to the recorded brake-pedal signals for each trial, in order to determine the average duration and shape of each brake adjustment. When the signals were extracted from the data, the parameters of G were manually set to fit the shape of the average brake-pedal adjustment (see Table 2).

3) CONTROLLED SYSTEM

The coefficients q_1 and q_2 were estimated by fitting the model described in (16) to the recorded data using the MATLAB function *fit*. Only the data in which drivers were braking and the vehicle was moving were retained.

D. EVALUATION OF DRIVER MODEL PERFORMANCE

The driver model was evaluated with a leave-one-out cross-validation process (LOOCV): for the entire dataset, each trial was left out once while the model was optimised using the remaining trials, and then the left-out trial was replayed using the optimised driver model together with the vehicle model. The outcome of each simulated trial was then compared with its observed counterpart by means of the following four metrics: 1) the time-to-arrival at the intersection point at brake onset (TTA_{BO}), 2) minimum acceleration (a_{min}), 3) maximum brake-pedal deflection (bp_{max}), and 4) the speed reduction (ΔV) from the vehicle speed at $t_{visibility}$ to the minimum speed.

The results for the first metric, TTA_{B0}, were compared to the BOP model detailed in Boda *et al.* [6]. The error distributions between the predicted and observed brake onsets for both the BOP model and the present implementation of the driver model were calculated.

The simulation results for the other metrics were compared against the observed data and classified into four categories: 1) *true positive* when a braking action was present in both the simulated and observed trials, 2) *false positive* when a braking action was present in the simulated trial but not in the

TABLE 3. Model parameters after optimisation.

Variable	$K_{excitatory}$	$k_{excitatory}$	$gate$	$k_{inhibitory}$
Estimate	1.49	4.66	0.69	-1.42
Standard error	0.033	0.293	0.076	0.068
p-value	< 0.01	-	-	< 0.01
Standard deviation due to random effect	0.18	0.644	-	0.24
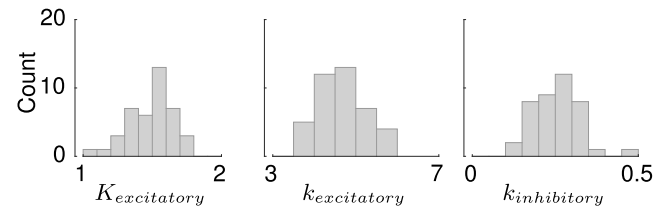
FIGURE 7. Distribution of the gain values of each driver (n = 41): $K_{excitatory}$, $k_{excitatory}$, and $k_{inhibitory}$.
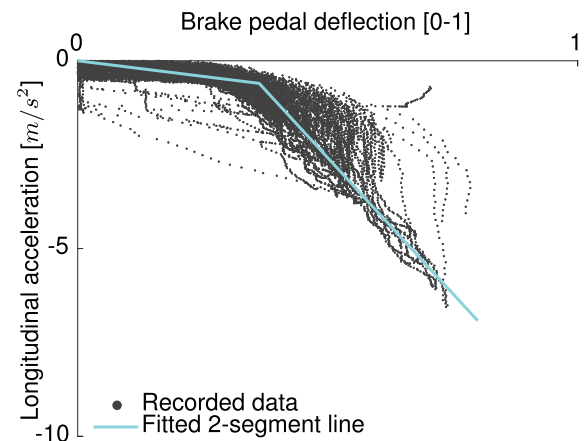
FIGURE 8. Observed longitudinal acceleration given brake-pedal deflection (dark-grey dots); the blue two-segment line was fitted to the data, simulating the car's acceleration level as a function of the brake-pedal deflection.

the observed trial, 3) *false negative* when a braking action was not present in the simulated trial but was present in the observed trial, and 4) *true negative* when no braking action was present in either trial.

III. RESULTS
A. OPTIMISATION OF MODELS
After data exclusion due to low-quality data or drivers failing to follow the instructions, 613 trials from 41 different drivers were considered for the model optimisation. The results of the optimisation are reported in Table 3, and the distribution of the gains for each driver are reported in Fig. 7.

The parameters of the vehicle model were estimated using 37,200 data points extracted from the time series (see Fig. 8). The fit returned $q_1 = -1.657$ and $q_2 = -14.46$.

TABLE 4. Performance ratios predicting whether drivers would apply braking for both the driver model and the BOP model.

	Driver model	Brake onset model
Sensitivity	0.981	1.000
Specificity	0.303	0.000
Precision	0.909	0.876
Accuracy	0.897	0.876
Fall-out	0.697	1.000
Miss rate	0.019	0.000

B. EVALUATION OF DRIVER MODEL PERFORMANCE: CROSS-VALIDATION

This section reports the results of the comparisons between the simulated and observed brake initiation times (TTA_{BO}) and the other metrics (a_{min}, bp_{max}, and ΔV).

1) BRAKE INITIATION

The observed TTA_{BO}, the TTA_{BO} predicted by the driver model, and that predicted by the BOP model are reported in Fig. 9. The scatter plot shows that the TTA_{BO} predicted by the BOP model was not able to reproduce the variability present in the observed TTA_{BO}. On the other hand, the driver model's predicted TTA_{BO} generated a variability close to that of the observed data. While the two models' error distributions have an equivalent standard deviation (1.685 for the driver model and 1.686 for the BOP model), the BOP model's distribution is shifted towards the negative values (mean $= -0.386$ s, and median $= -0.230$ s). In contrast, the error distribution for the driver model is more centred on zero (mean $= -0.202$ s, and median $= -0.008$ s). The results suggest that the driver model tends to predict a brake initiation closer to the observation than the BOP model does, since it predicts a later brake initiation.

The aforementioned results compared the brake initiation timings in the *true positive* predictions for both models. To evaluate how well the model predicted whether the drivers would brake or not, the ratios sensitivity, specificity, precision, accuracy, fall-out, and miss rate were calculated (see Table 4). Both models are comparable for sensitivity, precision, accuracy, and miss rate. For the specificity and the fall-out metrics, the driver model performed better than the BOP model. Thus it appears that the inhibitory cue introduced in our driver model caused it to perform better than the BOP model at predicting that no braking control would be applied. Finally, while the specificity is higher for the driver model, its value is still quite low (0.303), which can be explained by the fact that several drivers used engine braking instead of the brakes to regulate the car speed (resulting in numerous *false positives*).

2) TIME SERIES-RELATED METRICS

The predicted metrics related to the vehicle kinematics a_{min} and ΔV, as well as the driver input bp_{max}, were reported
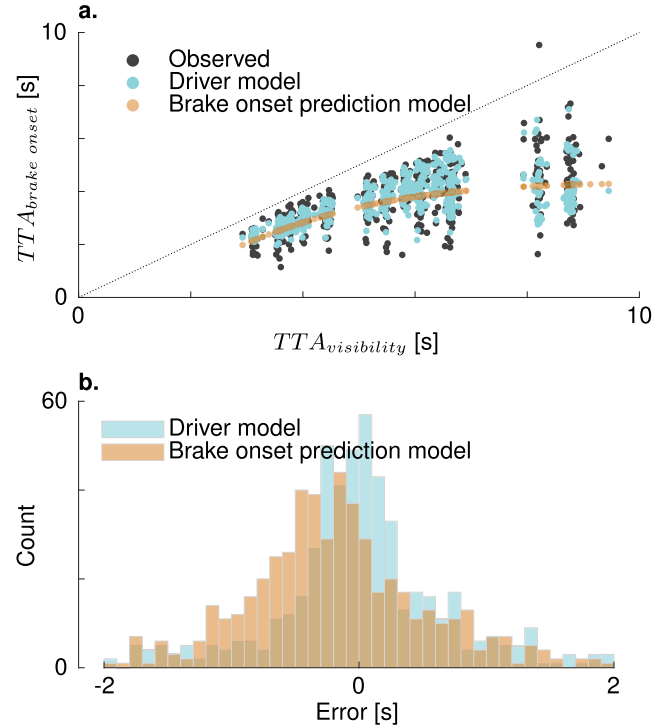
FIGURE 9. Comparison between observed and predicted brake onsets for both the driver model and the BOP model [6]: a) scatter plot showing the relationship between TTA_{BO} and $TTA_{visibility}$; b) histograms of the error between predicted and observed TTA_{BO}s for both models.

in Fig. 10., in the top row, the simulated values are plotted against the observed values. In the bottom row, the distributions of the error between the simulated and observed values are represented as histograms. For all plots, the data were classified into the four categories indicating whether the driver model correctly predicted whether the original driver braked. The mean, median, and standard deviation of each distribution are reported in Tables 5-6.

a: TRUE POSITIVES

The error distributions for the three metrics show that the simulated trials resulted in harder deceleration and greater speed reduction: for the majority of trials, the predicted a_{min} values were lower than their corresponding observed values ($median = 0.18 m/s^2$). However, for the trials with a high value for a_{min} (i.e., close to $0 m/s^2$), the predictions were quite similar to the observations. The same can be said for ΔV: for the values close to $0 m/s$, the predicted ΔV values were close to the observed values.

b: TRUE NEGATIVES

It is straightforward that the values of the metric bp_{max} from the simulated and observed data are similar for *true negative* predictions, since there was no braking. However, from the other metrics, it appears that in some trials, the drivers did decelerate without using the brake pedal (using engine braking instead).

TABLE 5. Distribution parameters for the error between the predicted and observed minimum accelerations (a_{min}), in m/s^2.

Category	Mean	Median	Standard deviation
true positive	0.00	0.18	3.37
true negative	-0.61	-0.59	0.17
false positive	0.54	0.08	1.35
false negative	-1.03	-0.88	0.46

TABLE 6. Distribution parameters for the error between the predicted and the observed speed reductions (ΔV), in [m/s].

Category	Mean	Median	Standard deviation
true positive	0.26	0.25	2.20
true negative	-0.27	-0.11	0.36
false positive	1.00	0.27	2.75
false negative	-1.39	-1.28	0.87

c: FALSE POSITIVES

The error distribution of bp_{max} was significantly larger for the predictions than the observations. However, the two other metrics show that the predicted values are not that different from the observed values. These similarities are the result of a very brief brake pedal adjustment, predicted by the model, that decelerated the vehicle only shortly (i.e., the predicted and observed ΔV values were similar). Additionally, as in the *true-negative* category, drivers seem to have decelerated their car using engine braking (while partially or fully releasing the gas pedal). Finally, there are three obvious outliers in the observed data (see Fig. 10.a and c); these three were, in fact, near-crash situations. The participants decided to cross the intersection in front of the bicycle even though the PET_{proj} margin was small, resulting in a large difference between the predictions and the observations because the driver model predicted safer behaviour. The predicted control was a result of fitting the driver model on multiple trials for each driver, producing an average behaviour that was safer than those outlier trials. Note that if the average behaviour of the driver had been unsafe (i.e., small PET_{proj} margin), it is likely that the driver model would have predicted an unsafe control.

d: FALSE NEGATIVES

Only ten cases were classified as false negatives. The median error and standard deviation of each metric are low, suggesting that in those observed trials the participants may have briefly braked. The situations may not have been very critical, so the driver model predicted that braking was not necessary. In other words, the model did not accumulate enough excitatory evidence before accumulating enough inhibitory evidence (i.e., $A_{inhibitory}$ reached -1 before $A_{excitatory}$ reached 1), resulting in an inhibition of the need for braking.

IV. DISCUSSION

The three objectives of this paper were 1) to present a computational model that can predict drivers' braking control when a cyclist crosses their travel path, 2) to evaluate its performance, and 3) to verify our hypothesis that the

TABLE 7. Distribution parameters for the error between the predicted and the observed maximum brake-pedal deflections (bp_{max}), ranging from 0 to 1 (where 1 is fully depressed).

Category	Mean	Median	Standard deviation
true positive	-0.07	-0.07	0.08
true negative	0.01	0.01	0.00
false positive	-0.36	-0.34	0.12
false negative	0.29	0.31	0.10

longitudinal looming and the projected post-encroachment time could explain drivers' braking control in this scenario.

A. MODEL PERFORMANCE

Overall, the results of the LOOCV process suggest that the current driver model was accurate at predicting brake-pedal control, not only at the moment when the driver initiates braking (as the BOP model does), but also during the subsequent period of braking control (until the final brake-pedal release). Hence, compared to the models of Silvano *et al.* [4] and Bella and Silvestri [5], this driver model goes further because it can provide a continuous prediction of driver control. This driver model also demonstrates that Markkula *et al.*'s modelling framework can be used to predict driver control in lateral interactions. Thus, our model complements other previous implementations (e.g., rear-end collision [9] or steering control [7]). Furthermore, the calculated sensitivity and specificity of the model indicate that it can predict brake initiation more accurately than the BOP model can. However, the specificity was quite low, perhaps because the participants used engine braking to regulate their speed instead of the brakes. Since engine braking was not implemented in the model, the model predicted braking instead, as compensation. In most cases, the predicted and observed speed reductions were actually quite similar. Future developments of the model should implement engine braking control to make it more realistic and improve the predictions.

The analysis of the metrics characterising brake pedal regulation after brake initiation (i.e., a_{min}, bp_{max}, and ΔV) showed that the model was able to predict braking control similar to that observed during the experiment. When drivers needed to brake significantly, the model had a tendency to predict even harder braking, resulting in a lower value for a_{min} and a greater speed reduction. This tendency could be caused by a combination of 2 factors: 1) the simplistic vehicle-dynamics model (see Fig. 8), and 2) the optimisation of $k_{excitatory}$, which was based only on the brake onset and not on the subsequent brake adjustments. To address the first factor, further development should consider implementing a more realistic vehicle-dynamics model. The second factor could be addressed by using all the brake adjustments in the optimisation process, but this would require a great deal of computing power, as well as a more refined algorithm to detect all the adjustments in the collected data.
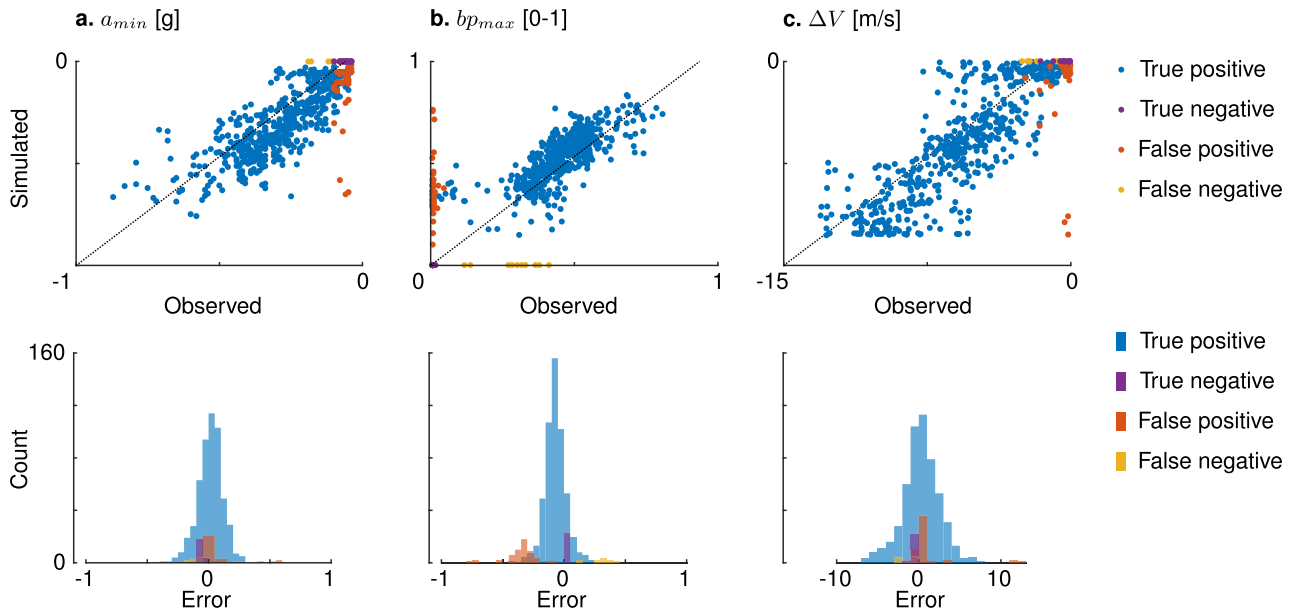
FIGURE 10. Driver model evaluation metrics. The top row comprises graphs of the simulated metrics against the observed metrics for all trials. The bottom row represents the histograms of the error (difference) between the simulated and observed metrics for all trials. For all graphs, the data were classified into four categories based on the brake onset prediction: 1) true positive, 2) true negative, 3) false positive, and 4) false negative. The left column represents the minimum acceleration reached during the trial (a_{min}), the middle column represents the maximum brake-pedal deflection (bp_{max}), and the right column represents the car's speed reduction from the time when the bicycle was visible for the first time to the minimum speed reached during the trial (ΔV).

B. MODEL IMPLEMENTATION AND PRACTICAL APPLICATIONS

The choice of the two input variables (i.e., the longitudinal looming and the projected post-encroachment time) was inspired by the human locomotion literature [13]. The performance assessment of the model suggests that the choice was adequate: those cues seemed to explain how drivers control their car when interacting with a crossing cyclist. However, it is unlikely that they are the only ones on which driver control depends. Therefore, when applying the driver model, researchers should consider other cues or mental states that might influence drivers' control. For example, because of the configuration of the experiment in the present implementation, the participants were surely attentive; therefore, the model may not correctly predict drivers' response processes when they are inattentive. The same limitation holds for other mental states, such as fatigue or cognitive load.

The driver model's inability to account for mental states may be problematic for counterfactual simulations, since they are an essential part of those simulations [20]. However, the driver model would still be relevant for threat-assessment algorithms for safety system activation. In a driving situation where a fully attentive driver would have already reacted, but the current driver has not initiated any response, it is likely that the safety system would have to issue a warning or even take over the car controls [21]–[23].

C. LIMITATIONS AND FUTURE RESEARCH

The main limitations of this work were the focus of the model on brake-pedal control and the simplifications that were made to be able to perform the modelling.

Modelling only brake-pedal control means, obviously, that the model could not predict other types of control (e.g., engine braking, steering, or acceleration). In fact, there were multiple trials in which drivers used engine braking, which seemed to be an actual strategy to regulate speed with a mild deceleration. However, engine braking was not modelled. Similarly, steering wheel control was not modelled, even though it is another important control that drivers can use to avoid a potential crash (i.e., steering to effect a change in bearing angle could increase the PET). Finally, gas-pedal control is also important, since it enables drivers to regulate their speed and, potentially, increase their PET (i.e., increasing their safety margins by speeding up when crossing the intersection in front of the bicycle, or by slowing down slightly when crossing after the bicycle). Furthermore, modelling the gas pedal may be important for indicating to safety systems that the driver has registered the presence of the cyclist and will act appropriately. Modelling gas-pedal control was also beyond the scope of this implementation.

The simplifications to the vehicle-dynamics model may have led to a wider variance in the error distributions. Introducing a more realistic model is likely to improve its prediction performance. Additionally, by manually tuning the motor-primitive G function, we may have generated a discrepancy between observed and simulated brake-pedal control. Another assumption was that the drivers' eye height is 1.2 m (instead of using the actual height for each drive); this may have led to overestimating or underestimating the value of τ^{-1}. As a result, the model may have produced less accurate predictions. Future research may address these limitations and simplifications, improving the model's suitability

for different applications as well as its prediction performance (e.g., future improvements of this model may combine machine learning approaches with the accumulation framework used in this paper). Furthermore, three near-crash situations in the data demonstrated that the model was not able to reproduce the participants' control in all cases. Therefore, the model requires further improvement so that it can describe driver behaviour that leads to a critical situation. More data on critical situations need to be collected to facilitate future development.

V. CONCLUSIONS

The leave-one-out cross-validation process showed that the computational driver model performed well at predicting driver control, whether the cyclist crossed the driver's travel path or not. The use of cues derived from the traffic conflict technique literature and the human locomotion literature enabled Markkula *et al.*'s modelling framework to be used for the first time to predict driver control in a lateral interaction. Furthermore, unlike previous driver models in similar traffic situations, the present driver model was able to predict continuous driver control. This computational model can be applied in safety systems' threat-assessment algorithms as well as in counterfactual simulations. However, before being used in production, the driver model would have to be validated with, for instance, naturalistic driving data. Furthermore, the prediction performance would have to be assessed on a wider range of kinematics, including factors such as engine braking or steering control, which could be modelled as a future development step toward reproducing more realistic driver control.

ACKNOWLEDGEMENTS

REFERENCES

[1] *Traffic Safety Basic Facts on Cyclists*, European Commission, Brussels, Belgium, Jun. 2017.

[2] *Euro NCAP Assessment Protocol AEB VRU Test Protocol v2.0.4*, Euro NCAP,, Leuven, Belgium, Feb. 2019.

[3] J. Dahl, G. R. de Campos, C. Olsson, and J. Fredriksson, "Collision avoidance: A literature review on threat-assessment techniques," *IEEE Trans. Intell. Veh.*, vol. 4, no. 1, pp. 101–113, Mar. 2019.

[4] A. P. Silvano, H. N. Koutsopoulos, and X. Ma, "Analysis of vehicle-bicycle interactions at unsignalized crossings: A probabilistic approach and application," *Accident Anal. Prevention*, vol. 97, pp. 38–48, Dec. 2016.

[5] F. Bella and M. Silvestri, "Driver–cyclist interaction under different bicycle crossroad configurations," in *Advances in Human Aspects of Transportation* (Advances in Intelligent Systems and Computing), N. A. Stanton, Ed. Cham, Switzerland: Springer, 2018, pp. 855–866.

[6] C.-N. Boda, M. Dozza, K. Bohman, P. Thalya, A. Larsson, and N. Lubbe, "Modelling how drivers respond to a bicyclist crossing their path at an intersection: How do test track and driving simulator compare?" *Accident Anal. Prevention*, vol. 111, pp. 238–250, Feb. 2018.

[7] G. Markkula, E. Boer, R. Romano, and N. Merat, "Sustained sensorimotor control as intermittent decisions about prediction errors: Computational framework and application to ground vehicle steering," *Biol. Cybern.*, vol. 112, no. 3, pp. 181–207, Jun. 2018, doi: 10.1007/s00422-017-0743-9.

[8] B. A. Purcell, R. P. Heitz, J. Y. Cohen, J. D. Schall, G. D. Logan, and T. J. Palmeri, "Neurally constrained modeling of perceptual decision making," *Psychol. Rev.*, vol. 117, no. 4, pp. 1113–1143, 2010.

[9] M. Svärd, G. Markkula, J. Engström, F. Granum, and J. Bärgman, "A quantitative driver model of pre-crash brake onset and control," *Proc. Hum. Factors Ergonom. Soc. Annu. Meeting*, vol. 61, no. 1, pp. 339–343, Sep. 2017.

[10] D. D. Salvucci and R. Gray, "A two-point visual control model of steering," *Perception*, vol. 33, no. 10, pp. 1233–1248, Oct. 2004, doi: 10.1068/p5343.

[11] G. Markkula, R. Romano, R. Waldram, O. Giles, C. Mole, and R. Wilkie, "Modelling visual-vestibular integration and behavioural adaptation in the driving simulator," 2018, *arXiv:1810.12441*. [Online]. Available: http://arxiv.org/abs/1810.12441

[12] Q. Xue, G. Markkula, X. Yan, and N. Merat, "Using perceptual cues for brake response to a lead vehicle: Comparing threshold and accumulator models of visual looming," *Accident Anal. Prevention*, vol. 118, pp. 114–124, Sep. 2018. [Online]. Available: http://www.sciencedirect.com/science/article/pii/S0001457518302239

[13] B. Fajen, "Guiding locomotion in complex, dynamic environments," *Frontiers Behav. Neurosci.*, vol. 7, p. 85, 2013. [Online]. Available: https://www.frontiersin.org/article/10.3389/fnbeh.2013.00085, doi: 10.3389/fnbeh.2013.00085.

[14] J. E. Cutting, P. M. Vishton, and P. A. Braren, "How we avoid collisions with stationary and moving objects," *Psychol. Rev.*, vol. 102, no. 4, p. 627, 1995.

[15] B. R. Fajen and W. H. Warren, "Visual guidance of intercepting a moving target on foot," *Perception*, vol. 33, no. 6, pp. 689–715, Jun. 2004, doi: 10.1068/p5236.

[16] B. L. Allen, B. T. Shin, and P. J. Cooper, "Analysis of traffic conflicts and collisions," Transp. Res. Board, Washington, DC, USA, Tech. Rep. 0361-1981, 1981.

[17] E. Rosén, J. Lang, and O. Bostrom, "Tests of sensors in line with proposed Euro NCAP procedure," in *Proc. 11th Int. Symp. Exhib. Sophisticated Car Occupant Saf. Syst. (Airbag)*, 2012.

[18] S. Schaal, S. Kotosaka, and D. Sternad, "Nonlinear dynamical systems as movement primitives," in *Proc. IEEE Int. Conf. Humanoid Robot.*, 2000, pp. 1–11.

[19] S. Dégallier Rochat, "Discrete and rhythmic motor primitives for the control of humanoid robots," Ph.D. dissertation, Dept. BIOROB–Biorobot. Lab., EPFL, Lausanne, Switzerland, 2010. [Online]. Available: http://infoscience.epfl.ch/record/150469/files/EPFL_TH4819.pdf

[20] J. Bärgman, C.-N. Boda, and M. Dozza, "Counterfactual simulations applied to SHRP2 crashes: The effect of driver behavior models on safety benefit estimations of intelligent safety systems," *Accident Anal. Prevention*, vol. 102, pp. 165–180, May 2017.

[21] M. Brännström, F. Sandblom, and L. Hammarstrand, "A probabilistic framework for decision-making in collision avoidance systems," *IEEE Trans. Intell. Transp. Syst.*, vol. 14, no. 2, pp. 637–648, Jun. 2013.

[22] G. R. de Campos, A. H. Runarsson, F. Granum, P. Falcone, and K. Alenljung, "Collision avoidance at intersections: A probabilistic threat-assessment and decision-making system for safety interventions," in *Proc. 17th Int. IEEE Conf. Intell. Transp. Syst. (ITSC)*, Oct. 2014, pp. 649–654.

[23] G. R. de Campos, F. D. Rossa, and A. Colombo, "Safety verification methods for human-driven vehicles at traffic intersections: Optimal driver-adaptive supervisory control," *IEEE Trans. Human-Mach. Syst.*, vol. 48, no. 1, pp. 72–84, Feb. 2018.

CHRISTIAN-NILS BODA received the M.Sc. degree in automotive engineering from the Chalmers University of Technology, Gothenburg, Sweden, and the M.Sc. degree in engineering science and mechanical engineering from Arts et Métiers ParisTech, Aix-en-Provence, France, in 2013. He is currently pursuing the Ph.D. degree in driver behaviour analysis and modeling with the Chalmers University of Technology. His Ph.D. work is part of the Drivers in Interaction with Vulnerable Road Users (DIV) project with Veoneer and Toyota Motor Europe as partners. His main research interest includes analysis and the computational modeling of driver behaviour when interacting with vulnerable road users.

ESKO LEHTONEN received the Ph.D. degree in cognitive science from the University of Helsinki, in 2014. He was a Postdoctoral Fellow with the University of Waikato, New Zealand, in 2017. From 2017 to 2019, he was a Postdoctoral Researcher with the Crash Analysis and Prevention Group, Chalmers University of Technology, Gothenburg, Sweden. He currently works as a Research Scientist with the VTT Technical Research Centre of Finland. His research has been concerned with human factors of road transport. He is interested in applying computational models to understand road user behaviour.

MARCO DOZZA received the Ph.D. degree in bioengineering from the University of Bologna, Italy, in collaboration with Oregon Health and Science University, Portland, OR, USA, in 2007. He worked as a System Developer for over two years with Volvo Technology, a research and innovation company inside the Volvo Group. Since 2009, he has been with the Chalmers University of Technology, Gothenburg, Sweden, where he is currently a Professor and leads the Crash Analysis and Prevention Unit. He is also an Examiner for the course active safety in the master's programme of automotive engineering. He is also working with SAFER, the Vehicle and Traffic Safety Center, Chalmers.

● ● ●